The Astrophysical Journal, 798:105 (10pp), 2015 January 10 doi:10.1088/0004-637X/798/2/105

TOWARD AN EMPIRICAL THEORY OF PULSAR EMISSION. X. ON THE PRECURSOR AND POSTCURSOR EMISSION

Rahul Basu[1,2], Dipanjan Mitra[1], and Joanna M. Rankin[3]
[1] National Centre for Radio Astrophysics, P.O. Bag 3, Pune University Campus, Pune 411 007, India
[2] Kepler Institute of Astronomy, University of Zielona Góra, Lubuska 2, 65-265 Zielona Góra, Poland; rahul@astro.ia.uz.zgora.pl
[3] Department of Physics, University of Vermont, Burlington, VT 05401, USA
Received 2014 September 8; accepted 2014 October 30; published 2015 January 6

ABSTRACT

Precursors and postcursors (PPCs) are rare emission components, which appear beyond the main pulse emission, in some cases far away from it, and are detected in a handful of pulsar. In this paper we attempt to characterize the PPC emission in relation to the pulsar main pulse geometry. In our analysis we find that PPC components have properties very different from that of outer conal emission. The separation of the PPC components from the main pulse center remains constant with frequency. In addition the beam opening angles corresponding to the separation of PPC components from the pulsar center are much larger than the largest encountered in conal emission. Pulsar radio emission is believed to originate within the magnetic polar flux tubes due to the growth of instabilities in the outflowing relativistic plasma. Observationally, there is strong evidence that the main pulse emission originates at altitudes of about 50 neutron star radii for a canonical pulsar. Currently, the most plausible radio emission model that can explain main pulse emission is the coherent curvature radiation mechanism, wherein relativistic charged solitons are formed in a non-stationary electron–positron-pair plasma. The wider beam opening angles of PPC require the emission to emanate from larger altitudes as compared to the main pulse, if both these components originate by the same emission mechanism. We explore this possibility and find that this emission mechanism is probably inapplicable at the height of the PPC emission. We propose that the PPC emission represents a new type of radiation from pulsars with a mechanism different from that of the main pulse.

Key word: pulsars: general

1. INTRODUCTION

Pulsar emission is comprised of periodic pulses with varying shapes and intensities. The integrated profile obtained by averaging a number of such pulses in phase (usually a few thousand pulses) is usually a stable feature showing little variation over time. This pulsed emission usually has a high degree of linear polarization with the polarization position angle (PPA) rotating across the profile with a characteristic S-shaped curve. Such radio emission is thought to originate within the open magnetic field lines above the polar cap, centered around the magnetic axis, and is highly beamed. The pulsar profile consists of one or more features, known as components, that exhibit many different configurations and in certain cases frequency evolution. The morphology and polarization properties of pulsar profiles are useful for determining the geometrical orientations of pulsars, the structure of their emission regions, their radio emission mechanisms, etc.(Lyne & Manchester 1988; Rankin 1983, 1990, hereafter ET I, ET IV).

An empirical beam model for the main pulse radio emission has emerged as a result of a wide array of studies conducted in the decades following the discovery of pulsars (ET IV; Rankin 1993a, hereafter ET VIa; Rankin 1993b, hereafter ET VIb; Mitra & Rankin 2002, hereafter ET VII; Mitra & Deshpande 1999; Gil & Sendyk 2000; Mitra & Li 2004). The main pulse emission consists in general of a central core component surrounded by nested inner and outer cones of emission. The rotating-vector model (RVM; Radhakrishnan & Cooke 1969), which states that the plane containing the magnetic field lines and the rotation axis determines the orientation of the emitted radiation, accounts for the S-shaped swing of the PPA. The core and the inner cone inhabit the regions of steeper PPA gradient, where the steepest gradient (SG) point is believed to fall near the longitude of the magnetic axis. The outer conal emission occupies the profile wings with a relatively flat PPA. The core and inner cones show nearly constant widths[4] and separations in most cases, whereas the outer conal emission exhibits radius-to-frequency mapping that shows increasing separation with decreasing frequency (ET VII). The polarization and spectral properties hint at two possibilities for the location of the outer and inner cones and core; either the different emission components originate near the outer magnetic flux tube boundary in which case they are emitted at successively lower heights, or they arise from similar heights but occupy ever more central regions of the flux tube. Gangadhara & Gupta (2001) used aberration retardation effects to question the viability of the first possibility while a more theoretical approach to explaining the emission prefers the later one (Maciesiak et al. 2012). The intensity of the various emission components varies, with one or more being weak or absent in certain pulsars and at high or low frequency, leading to asymmetric profiles known as "partial cones" (Lyne & Manchester 1988; Mitra & Rankin 2011, hereafter ET IX).

The precursor and postcursor (PPC) emission found in a small sample of pulsars is noteworthy owing to their nonconformity with well understood conceptions of profile structure, such as the empirical core/double-cone model outlined above. A precursor appears to be a distinct emission feature preceding the main pulse emission, whereas a postcursor follows it. These PPC features are found further away from the main pulse center as indicated by the PPA traverse wherein the SG point falls within the main pulse. The PPCs also exhibit a high degree of linear

[4] The core reflecting the angular width of the polar cap at the stellar surface.

polarization and a relatively flat PPA, and thus resemble the outer conal emission. However, unlike outer conal component pairs, they are always asymmetric with respect to the main pulse profile center. The presence of such PPCs has been reported in pulsars B0943+10 and B1822−09 by Backus et al. (2010) and also in B1322+83 and B2224+65 by ET IX, where in each case they fall adjacent to a main pulse, consistent with the above empirical model. To our knowledge no previous study has been conducted to investigate the properties and geometry of the PPC emission features. In this paper we endeavor to understand the location and physical properties of the PPC features within the context of the empirical beaming model developed in ET VIa, Mitra & Deshpande (1999), and ET VII. We have carried out a survey of the pulsar population to identify PPC features and studied their basic properties as a foundation for understanding them.

Section 2 reviews the quantitative geometry of the empirical core/double-cone emission beam model. Section 3 presents the results of our population survey wherein we attempt to distinguish PPC features from outer conal components. In Section 4 we investigate the implications of the PPC emission features from the perspective of their overall dipolar magnetic polar flux-tube geometry as a means of understanding their radio emission mechanism.

2. PULSAR EMISSION BEAM STRUCTURE

Pulsar radio emission originates within the polar flux tube of open dipolar field lines above the magnetic poles. The basic geometry of pulsar emission is determined by two angles: the so-called magnetic latitude angle between the rotation and magnetic axes α and the sightline impact angle between magnetic axis and observer's line of sight β. The RVM describes the PPA χ at any longitude φ in terms of this pulsar geometry as:

$$\tan\chi = \frac{\sin\alpha\sin\varphi}{\cos\alpha\sin(\alpha+\beta) - \sin\alpha\cos(\alpha+\beta)\cos\varphi}. \quad (1)$$

The SG point of the PPA, according to the RVM, is related to the geometry as:

$$\left(\frac{d\chi}{d\varphi}\right)_{\rm max} = \frac{\sin\alpha}{\sin\beta}. \quad (2)$$

It is possible to solve for the latitude angle α and impact angle β by carrying out RVM fits to the PPA traverse; however, the solutions are found to be highly correlated (Everett & Weisberg 2001). An independent means of estimating the latitude angle α was devised in ET IV using the half power widths, $W_{\rm core}$, of core emission components as (Maciesiak & Gil 2011):

$$\sin\alpha = 2.^{\circ}45\,P^{-0.5}/W_{\rm core}. \quad (3)$$

The polar flux-tube radius angle, ρ, delimiting the emission region can be estimated using the overall pulse width, W, and the basic pulsar geometry (Gil et al. 1984) as:

$$\sin^2(\rho/2) = \sin^2(\beta/2) + \sin\alpha\sin(\alpha+\beta)\sin^2(W/4). \quad (4)$$

A series of studies have been devoted to determining the beam opening angles of the conal emission, especially in pulsars with associated core emission, and ET VIa, ET VIb discovered that the conal emission beams consist of a pair of inner and outer cones. Mitra & Deshpande (1999) analyzed around 40 pulsars at 6 different frequencies and postulated the presence of 3 concentric conal beams with frequency evolution given as:

$$\rho^{\rm r}_{\rm MHz} = 4.^{\circ}8\varrho\left(1 + (66 \pm 10)\nu_{\rm MHz}^{-1\pm0.1}\right)P^{-0.5}, \quad (5)$$

with radii corresponding to $\varrho = 0.8, 1.0, 1.3$ to within error of 0.03.

The outermost conal emission seems to be associated with the last open magnetic field lines and thus provides direct estimates of the corresponding emission heights. Taking into account divergence of the dipolar magnetic field lines with frequency, the emission height r can be expressed in terms of the angular size of the polar cap on the pulsar surface (radius $1.^{\circ}24$), the radius of the neutron star R_S and the beam opening angle $\rho^{\rm outer}$.

$$r = \mathrm{P}\left(\frac{\rho^{\rm outer}}{1.^{\circ}24}\right)^2 R_S. \quad (6)$$

The main pulse emission based on the above geometrical analysis is estimated to arise at heights of about 20–50 R_S for a typical pulsar (ET VIa; Kijak & Gil 1998; ET VII). Emission-height estimates using aberration-retardation effects—i.e., conal component shifts relative to the profile center as a result of relativistic beaming, which are independent of the pulsar geometry—are consistent with those estimated using the basic geometry above (Blaskiewicz et al. 1991; Gangadhara & Gupta 2001; Krzeszowski et al. 2009).

3. PPC EMISSION AND WIDE PROFILES

We have conducted an extensive population survey to identify pulsars with broad, asymmetric profile features that might constitute PPC emission. This also led to the identification of some additional pulsars with "partial cones," which appear to be extreme examples of outer conal emission (ET IX). We investigated pulsar profiles at multiple frequencies using various archival sources (Gould & Lyne 1998; Seiradakis et al. 1995; Lorimer et al. 1995; Weisberg et al. 1999, 2004) as well as unpublished observations from Arecibo and the GMRT. The 14 pulsars we identified with putative PPC emission are listed in Table 1. The beam opening angles for the separation of candidate PPC features from the profile center were determined using 2 times the value of their separations from the main pulse centers. The extremity of the outer conal emission (Equation (5)) was used to distinguish between PPC and outer conal components (see Table 1). For three pulsars, B0940+16, J1332−3032, and B1822−14, no published emission geometry was available; however, we were able to estimate parameter for one of them and so carry out the above analysis. In the remainder of this section we describe each of the pulsars in more detail.

B0823+26 exhibits a well established postcursor feature in addition to its main pulse and interpulse (Hankins & Fowler 1986). Rankin & Rathnasree (1995) studied the pulsar's profile regions in detail and appeared to confirm an increasing postcursor separation with frequency. The basic geometry was modeled in ET VIb and the values reported in Table 1. Profiles for this pulsar including its postcursor have been measured over the frequency range from 317 MHz to 1.4 GHz and their various characteristics given in Table 2. The interpulse to main pulse separation is nearly 180° over this band, strongly suggesting an orthogonal geometry. However, we find that the postcursor is comprised of three features that have different spectra as shown in Figure 1. The leading feature is prominent at lower frequencies but hardly detectable above 1 GHz; thus use of the

Table 1
Emission Geometry and Beam Opening Angles at 1 GHz

Pulsar	Period (s)	Profile Class	α (°)	β (°)	Ref.	Separation (°)	$\rho P^{0.5}$ (°)	Comment
B0823+26	0.531	S_t	84	+1.9	1	41.6	30.2	Postcursor
B0940+16	1.087	D?	∼32	∼0		85	∼44	Postcursor?
B0943+10	1.098	S_d	11.6	4.31	2	52.3	13.2	Precursor
B0950+08	0.253	S_d	16	–11.3		150	10.2	Precursor
B1322+83	0.670	S_d	14	5.1	3	42.6	10.5	Precursor
J1332−3032	0.650	?	...	...		119.0	...	Precursor?
B1524−39	2.418	D	16.5	–0.4	5	57.7	12.5	Precursor
B1530+27	1.125	S_d/D	30	+4.9	3	52	29.2	Postcursor
B1742−30	0.367	T	24	6.4	3	14.3	5.5	Outer cone
B1822−09	0.769	T	86	0.0	4	14.3	12.5	Precursor
B1822−14	0.279	?	...	...		26.4	...	Precursor?
B1929+10	0.227	T/M?	90	41.8		115	51.6	Postcursor
B2217+47	0.538	S_t	42	4.5	3	42–68	23–35	Postcursor
B2224+65	0.683	$T_{1/2}$	15.2	3.3	5	30.1	7.6	Outer cone

Note. (1) ET VIb; (2) Rankin et al. (2003); (3) ET IX; (4) Backus et al. (2010); (5) this paper.

postcursor peak spacing leads to flawed conclusions about its frequency evolution. The trailing extremity of the postcursor provides a better estimator of its separation. In Table 2 we list the half widths of the main pulse, the separations of the postcursor feature (5σ at the outer edge) from the pulse center, and the beam opening angles for both main pulse and the postcursor separation at all available frequencies. Therefore, the postcursor separation does not appear to vary with frequency contrary to Hankins & Fowler (1986) and Rankin & Rathnasree (1995). The frequency evolution of the postcursor emission beam and the corresponding emission height using Equation (6) is shown in Figure 2.

B0940+16 shows what appears to be a postcursor, at 430 MHz, about 85° from the center of its main pulse (Deich 1986; Hankins & Rankin 2010). The feature is also present at 1.4 GHz (Weisberg et al. 1999), though it is much weaker. The PPA shows a relatively flat swing across the main pulse suggesting conal emission cut centrally by the sightline. We then tentatively class this pulsar as exhibiting an inner cone double profile with a β value near 0°, such that α would then be about 32°. The beam opening angle (normalized by the pulsar period) is around 44° (see Table 1) which lies outside the conal boundary.

B0943+10 is well known for its so-called quiescent (Q) and burst (B) modes, and its profile evolution and highly regular subpulse drifting in the latter establish it as a classic example of conal emission. Backus et al. (2010) discovered a profile feature leading the main pulse during only the Q mode that they identified as a precursor. We had access to Q-mode profiles at 325, 610, and 1391 MHz which were used for our investigation here. The pulsar is weaker during the Q mode, and adequately sensitive profiles at higher frequencies are difficult to obtain owing to its steep radio frequencies (RF) spectrum. ET VIb computed its basic geometry, but more accurate values come from more recent models of its subbeam carousel (Deshpande & Rankin 2001; Rankin et al. 2003), and these are the values reported in Table 1. We have determined the width of the main pulse, the separation of the precursor from the pulse center and the beam opening angles as shown in Table 2.

B0950+08 shows the presence of a leading component about 150° from the main pulse. This leading component has usually been considered an interpulse, and questions about whether the combination represented a nearly aligned or orthogonal rotator (one- or two-pole configuration) much debated (Blaskiewicz et al. 1991; ET VIb; Everett & Weisberg 2001). On its own, however, the evidence is strong that the main pulse represents an outer conal single geometry given the prominent bifurcation of its profile at low frequencies, e.g., Hankins & Rankin (2010). Moreover, the very shallow PPA rate and strong indication of a 360° traverse over each rotation (e.g., Blaskiewicz et al. 1991) almost definitively signals a small α and negative β similar to the calculations in ET VIa, ET VIb. The main pulse is joined to the preceding component via a bridge emission, which also shows high degree of linear polarization and is located far away from the SG (located close to the main pulse peak) suggesting a possible precursor emission. We used high quality GMRT and Arecibo data with frequencies ranging from 111 MHz to 2370 MHz, with the main pulse showing considerable profile evolution across frequencies. As a result it was difficult to identify the central point and we used the midpoint of the half widths as reference for determining the separation between components. The separation between the two components shows a slight frequency evolution and increases with increasing frequency (see Figure 1 and Table 2), which may be due to errors in determining the pulse center. We used the outer conal geometry as estimated by ET VIb (with correction of sign in β following the convention of Everett & Weisberg 2001) with values of $\alpha = 16°$ and $\beta = -11.^{\circ}3$. The period normalized beam width for the leading emission component at 1 GHz turns out to be 10° as seen in other precursors. The leading emission in this pulsar is then most likely a precursor but may show a slight frequency evolution.

B1322+83 was studied in detail in ET IX at 325 MHz, who interpreted its profile as having a precursor emission feature. The main pulse emission exhibits the properties of a conal single profile similar to the Q mode of B0943+10. The pulsar also shows signatures of interstellar scattering, which made estimating the feature widths difficult. The geometry of the pulsar was determined in ET IX (see Table 1). The precursor feature is particularly weak in this pulsar and was only detected at one other frequency, 610 MHz. We were unable to estimate the width of the precursor at 610 MHz due to its weakness, though

Table 2
The Component Spacing, Width, and Beam Radius

Pulsar	Period (s)	ν (MHz)	MP Width (°)	PC Width (°)	PC-MP Sep (°)	$\rho^{\rm MP}$ (°)	$\rho^{\rm PC}$ (°)
		317	5.4 ± 0.1	...	41.4 ± 0.4	3.3 ± 0.04	41.3 ± 0.1
		408	4.1 ± 0.1	...	42.8 ± 0.8	2.8 ± 0.04	42.7 ± 0.2
		430	4.1 ± 0.1	...	42.0 ± 0.4	2.8 ± 0.04	41.9 ± 0.1
B0823+26	0.531	591	5.0 ± 0.1	...	41.7 ± 0.7	3.1 ± 0.04	41.6 ± 0.2
		610	4.1 ± 0.1	...	41.2 ± 0.7	2.8 ± 0.04	41.1 ± 0.2
		1178	2.7 ± 0.1	...	41.4 ± 0.2	2.3 ± 0.03	41.3 ± 0.1
		1404	3.2 ± 0.1	...	42.1 ± 0.7	2.5 ± 0.03	42.0 ± 0.2
		1415	3.4 ± 0.1	...	41.8 ± 0.4	2.5 ± 0.03	41.7 ± 0.1
		325	12.8 ± 0.1	23.4 ± 1.0	52.8 ± 0.6	4.6 ± 0.05	12.7 ± 0.1
B0943+10	1.098	610	13.2 ± 0.2	14.4 ± 1.2	51.7 ± 0.7	4.6 ± 0.05	12.5 ± 0.1
		1391	15.2 ± 0.7	18.7 ± 1.0	50.2 ± 0.8	4.7 ± 0.05	12.3 ± 0.1
		111	19.7 ± 0.4	...	144.9 ± 0.9	11.4 ± 0.05	20.0 ± 0.1
		317	14.7 ± 0.4	25.2 ± 1.0	146.3 ± 0.4	11.4 ± 0.05	20.1 ± 0.1
B0950+08	0.253	430	14.1 ± 0.4	23.2 ± 1.1	147.3 ± 0.5	11.3 ± 0.05	20.1 ± 0.1
		602	12.3 ± 0.3	22.0 ± 1.0	149.1 ± 0.4	11.3 ± 0.05	20.2 ± 0.1
		1408	14.4 ± 0.4	15.8 ± 1.8	151.2 ± 0.4	11.4 ± 0.05	20.2 ± 0.1
		2307	12.7 ± 0.4	16.9 ± 1.1	153.5 ± 0.8	11.3 ± 0.05	20.3 ± 0.1
B1322+83	0.670	325	9.8 ± 0.2	17.1 ± 1.0	42.9 ± 0.6	5.3 ± 0.1	12.9 ± 0.1
		610	10.0 ± 0.4	...	42.2 ± 0.8	5.3 ± 0.1	12.7 ± 0.2
		243	8.1 ± 0.4	3.9 ± 0.6	14.4 ± 0.3	4.0 ± 0.2	14.4 ± 0.3
		325	7.1 ± 0.2	7.0 ± 0.2	15.2 ± 0.1	3.5 ± 0.1	15.2 ± 0.1
		408	6.7 ± 0.4	4.1 ± 0.2	14.8 ± 0.1	3.3 ± 0.2	14.8 ± 0.1
		610	7.1 ± 1.1	6.7 ± 0.2	14.6 ± 0.6	3.5 ± 0.5	14.6 ± 0.6
		800	6.8 ± 0.1	7.4 ± 0.3	14.5 ± 0.1	3.4 ± 0.1	14.5 ± 0.1
		925	5.4 ± 0.1	7.7 ± 0.2	15.0 ± 0.1	2.7 ± 0.1	15.0 ± 0.1
		1330	6.5 ± 0.1	7.1 ± 0.1	14.7 ± 0.1	3.2 ± 0.1	14.7 ± 0.1
B1822−09	0.769	1408	5.2 ± 0.1	6.0 ± 0.1	14.7 ± 0.1	2.6 ± 0.1	14.7 ± 0.1
		1408	5.5 ± 0.2	5.4 ± 0.1	14.6 ± 0.1	2.7 ± 0.1	14.6 ± 0.1
		1410	6.1 ± 0.3	5.6 ± 0.2	13.6 ± 0.1	3.0 ± 0.2	13.6 ± 0.1
		1640	5.7 ± 0.3	6.4 ± 1.0	14.9 ± 0.4	2.8 ± 0.2	14.9 ± 0.4
		1642	6.0 ± 1.1	5.6 ± 0.1	14.3 ± 0.8	3.0 ± 0.5	14.3 ± 0.8
		4750	5.9 ± 0.7	5.1 ± 0.1	14.1 ± 0.4	2.9 ± 0.3	14.1 ± 0.4
		4850	4.9 ± 0.1	5.6 ± 0.1	13.9 ± 0.04	2.4 ± 0.1	13.9 ± 0.04
		10450	3.0 ± 0.2	5.5 ± 0.5	14.3 ± 0.2	1.5 ± 0.1	14.3 ± 0.2
		10550	3.6 ± 0.1	6.3 ± 0.3	14.3 ± 0.1	1.8 ± 0.1	14.3 ± 0.1
		325	12.1 ± 0.2	18.7 ± 0.7	33.3 ± 0.3	3.7 ± 0.2	10.0 ± 0.1
		400	12.0 ± 0.2	15.1 ± 0.7	32.1 ± 0.3	3.7 ± 0.2	9.7 ± 0.1
		408	10.4 ± 0.3	13.4 ± 1.3	32.7 ± 0.6	3.6 ± 0.2	9.9 ± 0.2
		610	11.3 ± 0.2	10.9 ± 0.3	31.2 ± 0.1	3.7 ± 0.2	9.5 ± 0.1
B2224+65	0.683	800	12.0 ± 0.5	10.1 ± 0.4	30.5 ± 0.3	3.7 ± 0.2	9.3 ± 0.1
		925	11.3 ± 0.5	7.5 ± 0.3	29.9 ± 0.2	3.7 ± 0.2	9.2 ± 0.1
		1330	12.3 ± 0.3	8.3 ± 0.4	29.5 ± 0.2	3.7 ± 0.2	9.0 ± 0.1
		1408	10.7 ± 0.1	6.7 ± 0.1	29.5 ± 0.2	3.6 ± 0.2	9.0 ± 0.1
		1408	11.7 ± 0.2	7.0 ± 0.1	29.3 ± 0.1	3.7 ± 0.2	9.0 ± 0.1
		1642	11.5 ± 0.3	6.7 ± 0.1	28.9 ± 0.1	3.7 ± 0.2	8.9 ± 0.1

its peak could be identified. The main pulse and precursor widths and their separation at 325 and 610 MHz are shown in Table 2 along with the radius of the beam opening angles.

J1332−3032. The pulsar exhibits a two component profile at low frequencies < 1 GHz (325, 430 and 610 MHz). The leading component is 119° ahead of the main pulse emission with the separation remaining constant across frequencies and is therefore ostensible precursor emission. The pulsar is relatively weak and lacks polarization measurements at any of the frequencies. We do not have any estimate of the pulsar's geometry and this makes it difficult to distinguish between a wider inner cone and precursor emission.

B1524−39. appears to have an emission feature about 58° ahead of its main pulse. This putative precursor emission was detected only at 435 MHz and was not detected at 325 and 610 MHz. The main pulse profile has a conal double form with a steep 180° PPA sweep across it and shows little or no width evolution with frequency. The geometry of the pulsar was determined by fitting the RVM to the PPA at 325 MHz and is shown in Table 1. The beam opening angle for the separation of the precursor feature from the profile center was well outside the conal range (see Table 1). We note the peculiarity of the precursor detection at a single frequency and its absence at both 325 and 610 MHz. This suggests the possibility that the pulsar has modes like those of B0943+10 wherein precursor emission is present only during a certain emission mode. The pulsar needs to be observed for longer durations to assess whether mode changing could be an issue.

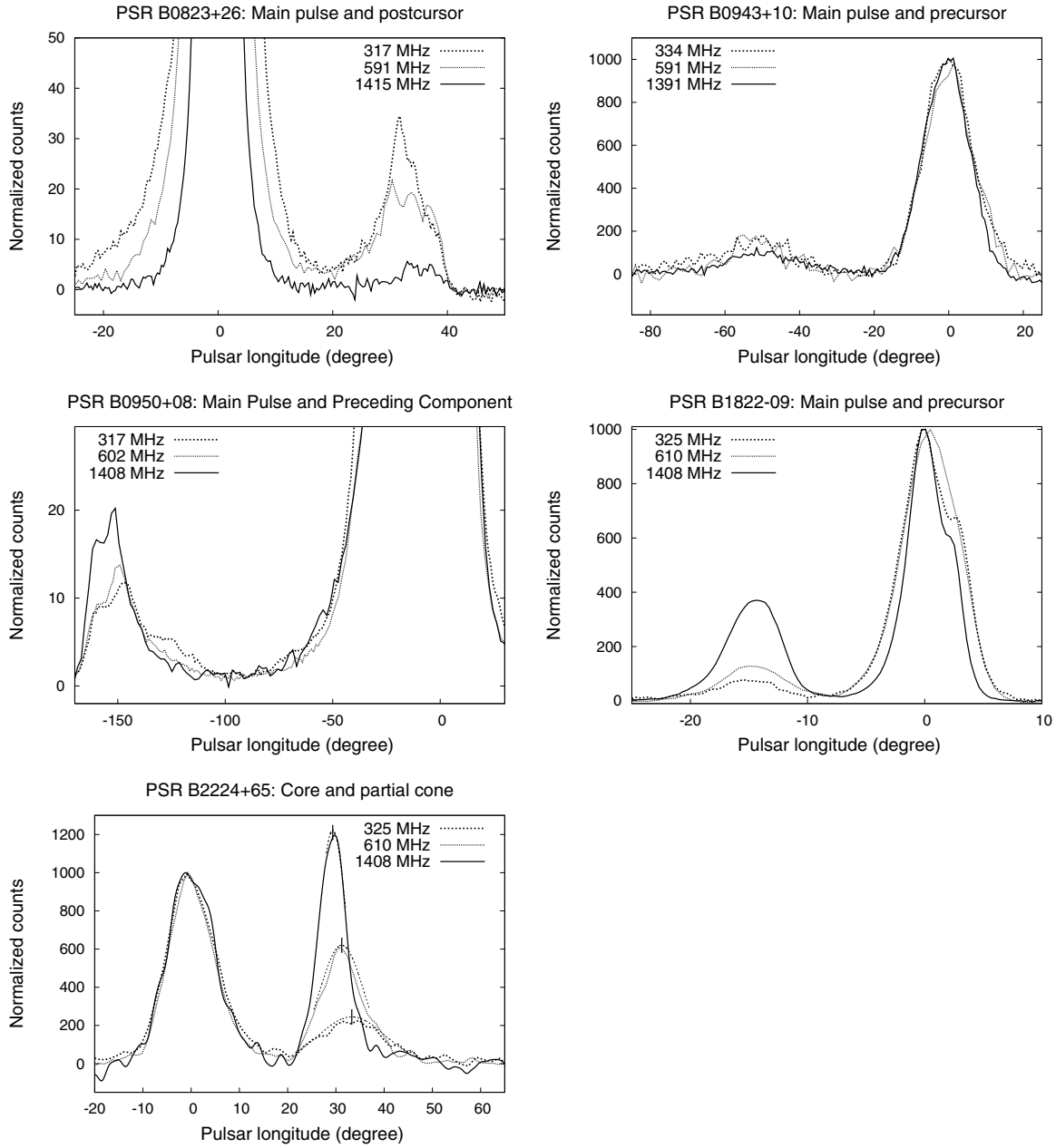

Figure 1. Frequency evolution of the postcursor in pulsar B0823+26 (top left), the precursor in B0943+10 (top right), the precursor in B0950+08 (middle left), the precursor in B1822−09 (middle right), and the ostensible partial cone in B2224+65 (bottom left). The precursors in B0943+10 and B1822−09 maintain a constant separation from the main pulse center with frequency. The precursor is brighter at higher frequencies in the case of B1822−09. The precursor remains more or less constant in B0943+10 in our frequency range; however, it is known to get considerably weaker at lower frequencies. The precursor in B0950+08 shows a slight evolution with frequency where the emission grows stronger and moves further away from the main pulse with increasing frequency. However, the main pulse in this pulsar also shows significant frequency evolution, and the perceived shift may be a result of erroneous determination of pulse center at each frequency. The postcursor in B0823+26 consists of three subfeatures, all of which grow weaker with increasing frequency. The leading feature is most prominent at 317 MHz and is barely detected at 1.4 GHz. However, the outer edge of the postcursor emission maintains a constant separation from the main pulse. The outer conal emission in B2224+65 which here is identified as a partial cone becomes more prominent with increasing frequency relative to the central core component (the latter typically have steeper RF spectra). The separation of the conal component from the pulse center as well as the component width decreases with increasing frequency.

B1530+27. shows weak putative postcursor emission 52° from its main pulse peak. The pulsar has been studied in detail at 325 MHz in ET IX where its main pulse was identified as conal. Its main pulse shows a double form and a shallow PPA traverse implying a probable oblique sightline cut through the emission beam. The above study also determined the pulsar's geometry, which is given in Table 1. The postcursor feature is also seen at 430 MHz (Weisberg et al. 2004) at the same separation from the main pulse. The beam opening angle for the separation of postcursor emission from the pulse center is shown in Table 1, which clearly lies outside the conal range.

B1742−30. A leading component located roughly 15° ahead of the main pulse is seen in this pulsar over a wide frequency range. The separation of this feature from the trailing components increases with wavelength. A low level counterpart trailing the central component is also visible in certain higher sensitivity profiles. The geometry of the pulsar was determined in ET IX and is shown in Table 1. The beam opening angle at 1 GHz for

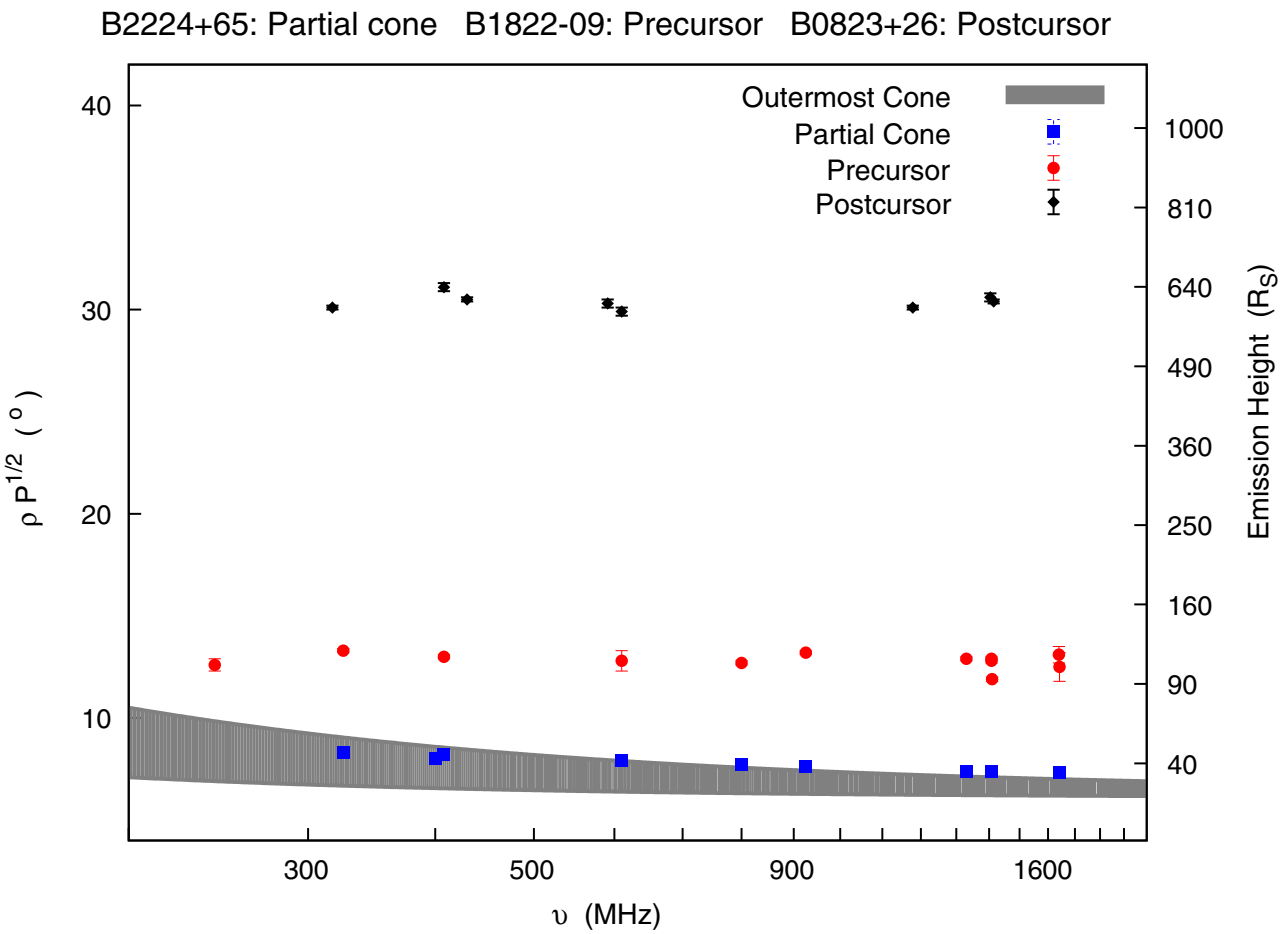

Figure 2. Evolution of the beam opening-angle radius with frequency for the precursor in B1822−09, postcursor in B0823+26, and the partial cone in B2224+65. The shaded region represents the outermost cone as shown in Equation (5) ($\varrho = 1.3$). The boundaries of the shaded region signify the maximum and minimum errors in determining the conal boundary. The partial cone component in B2224+65 exhibits decreasing separation from the pulse center with increasing frequency and has been identified as an extremely outer region of the beam and not a postcursor component. The precursor and postcursor components are not consistent with the core-cone morphology, showing no frequency evolution of separation and lie outside the conal beam opening angle. In the right hand side we have shown the emission heights for the beam radius corresponding to the last open magnetic field lines. The PPC components originate much higher up along the open field lines compared to the main pulse emission.

the separation of the leading component from the pulse center is calculated (see Table 1) and lies within the conal region as per Equation (5). The leading emission component is thus identified as outer conal in this pulsar which exhibits such an unusually broad triple (T) profile.

B1822−09's profile also famously exhibits both a leading precursor and an interpulse in addition to its main pulse, and these emission features are seen alternately in its quiescent (Q) and burst (B) modes. The interpulse appears in its Q mode and the precursor in the B. However, there are mixed-mode episodes where both emission components are present (or absent) simultaneously (Latham et al. 2012). Gil et al. (1994) studied this pulsar extensively at several frequencies, interestingly reporting microstructures in the leading feature, but failed to identify it as having the unique properties of a precursor. Backus et al. (2010) first established the core/inner cone character of the pulsar's main pulse in relation to the leading precursor feature. The geometry of this pulsar has been computed in ET IX and given in Table 1. We studied the pulsar over a wide frequency range from 240 MHz to 10.5 GHz with the various component widths and beam opening radii summarized in Table 2. The precursor emission becomes relatively weaker with decreasing frequencies (see Figure 1). The beam opening angle for the separation of precursor emission from pulse center lies well outside the conal region and does not evolve with frequency (see Figure 2).

B1822−14 shows an emission feature preceding its main pulse, faintly at 1.4–1.6 GHz and imperceptible below (Gould & Lyne 1998) but quite brightly at 5 GHz (von Hoensbroech 1999). No published geometry for the pulsar is available and the evidence is limited for us to characterize the main pulse as well as the leading component.

B1929+10's profile consists of a core/(double?)cone main pulse and a core-single interpulse. As discussed in ET VIa, ET VIb, the widths of both cores indicate an orthogonal (two-pole) geometry. The main pulse and interpulse are separated by "bridges" of weak highly linearly polarized emission over essentially the entire rotation cycle; however, a somewhat stronger postcursor feature follows the main pulse. The separation between the main pulse and interpulse is 187.°4 and remains constant with frequency (Hankins & Fowler 1986). At odds with this view are RVM fits to the "bridge" emission (that necessarily ignore the main pulse; Everett & Weisberg 2001) suggesting α and β values of some 36° and 26°. Given that these values permit no sense to be made of the ostensible T or M main-pulse component structure, we adopt the above two-pole geometry for

our purposes here (and wonder if the low level "bridge" emission has a different source). The pulsar's off-pulse emission has been studied in detail by Rankin & Rathnasree (1997). The putative postcursor component is fully linearly polarized, follows the main-pulse peak by around 115°, and its position seems to remain constant with frequency.

B2217+47. The presence of a postcursor component in this pulsar at 102.5 MHz was reported by Suleymanova & Shitov (1994). The postcursor was connected to the main pulse via an emission bridge and was distinguished by a gradual time evolution. Its intensity increased with time (during the observing cycle lasting several years), and it moved towards the main pulse resulting in a decreasing separation between the components. The temporal variations of the postcursor were attributed to precession of the rotation axis. The postcursor is absent in higher frequencies despite the presence of good quality profiles. The geometry of the pulsar has been determined in ET IX with the α and β values shown in Table 1. The main pulse is classified as core-single. The corresponding beam opening angle for the separation of the postcursor from pulse center has been determined in Table 1 and turns out to be large like other postcursor emission.

B2224+65 shows a profile with two widely separated emission components, and several studies have interpreted these differently: Lyne & Manchester (1988) classified the profile as being a "partial cone" while ET IX identified the trailing feature as a postcursor in relation to a core-single main pulse. The latter study estimated the geometry of the pulsar as having an α of 27° and β of 4.°9. The core component width (see Table 2 and Equation (3)) was incompatible with the above geometry. Using our measured core widths we established the corrected geometry for this pulsar to be $\alpha = 15.°2$ and $\beta = 3.°3$.[5] The pulsar was studied over frequencies ranging from 325 MHz to 1.6 GHz and the various component widths and beam opening angles are shown in Table 2. The trailing component grows stronger and its separation decreases with increasing frequency (see Figure 1). In addition the beam opening angles lie on the border of outer conal beam as seen in Figure 2. We identify the trailing component to be outer conal emission, a classic example of a partial cone, lying on the extreme edge of the emission beam.

4. DISCUSSION

4.1. Properties of PPC Emission

The PPC emission is asymmetric, without any counterpart at the opposite side of the pulse center, and thereby resembles a partial cone. It is generally connected to the main pulse with a low level emission bridge, and exhibits a high degree of linear polarization with a relatively flat PPA traverse. Our analysis, carried out assuming that all emission components originate along the open dipolar magnetic field lines, reveal the PPCs to be distinct from the outer conal emission, and we highlight some of their characteristic features.

Separation of components: PPC emission features, much like interpulses or inner conal component pairs, show little or no significant spectral change in their spacing from the main pulse region. This property serves to differentiate PPC features from outer conal component pairs, which regularly show the widening with wavelength known as "radius-to-frequency mapping." Interpulse and main pulse emission are expected to originate from opposite magnetic poles, with the interpulse visible only for pulsars with an orthogonal geometry. PPC emission is then quite unlike that from either polar flux tube, and it seems likely that it is emitted at some different location within the pulsar magnetosphere. However, given that the PPC-main pulse separations are usually much less than 180°, the PPC emission is likely to arise from the same magnetic pole as the main pulse.

Beam opening angle. Outer conal emission, to the extent that it originates near the periphery of the polar flux tube, represents the extremity of main pulse emission in terms of both opening angle and altitude. The beam opening angle changes with frequency and is estimated using the geometry of the pulsar and the longitudinal extent of the component in question (see Equation (4)). The upper limit for the width of a beam of outer conal emission turns out to be around 7.°5 at 1 GHz (Equation (5); here the beam radius is normalized by $P^{0.5}$). The partial cone in pulsar B2224+65 has a beam opening angle of 7.°6 and is consistent with the conal width. The precursor emission in B0943+10, B0950+08, B1322+83, B1524−39, and B1822−09 has beam opening angles between 10° and 15°, while the postcursor components in B0823+26, B1530+27, and B2217+47 have beam opening angles around 30°.[6] The beam opening angles based on the separation between the PPC and main pulse are much greater than the conventional outer conal emission and form the distinguishing feature between them. It is interesting to note that the beam radii of the PPC emission are different, with the latter values being greater by a factor of two. We have too few examples of PPC emission to draw any more general conclusion regarding their differences.

Emission heights. The radio emission in pulsars is expected to originate along the open dipolar magnetic field lines. The outer conal emission lies in the outermost regions of the emission beam and its beam opening angle provides an estimate of emission height. The emission heights using the minimum and maximum error values of outermost beam opening angles specified in Equations (5) and (6) turns out to be 25–35 R_S at 1 GHz for a 1 s pulsar. Using the beam opening angle the emission height for the precursor emission is calculated to be around 100 R_S and the postcursor emission is more than 500 R_S (see Figure 2). The above estimates should be taken as lower limits as we do not yet know the exact location of the PPC components within the emission beam. It is clear that the PPC emission has a location much higher up in the pulsar magnetosphere compared to the main pulse emission. The implications of the emission height on the underlying mechanism of emission are discussed in the next subsection.

Polarization characteristics. The PPC components of B0823+26, B0943+10, B1322+83, B1530+27, and B1822−09 with their polarization properties are shown in Figure 3. The polarization characteristics of the PPC emission in the well known pulsars B0950+08 and B1929+10 are shown in McLaughlin & Rankin (2000, see their Figures 4 and 5). The PPC emission is associated with a high degree of linear polarization greater than 70% in most cases. The circular polarization is much lower and is usually less than 20%. The notable exception being B1530+27 where the postcursor emission shows relatively low linear polarization, less than 30%, and high circular polarization, greater

[5] We used $(d\chi/d\varphi)_{\rm max} = -4.5$ from Lyne & Manchester (1988) in our calculations of β for the pulsar B2224+65.

[6] The beam opening angle of the postcursor in B1929+10 is around 50°, but this value is likely to be lower as we have used the most extreme case of orthogonal geometry for calculations; see Section 3 for details. Similarly, the large beam opening angle of the postcursor in B0940+16 may very well be due to errors in determining the pulsar geometry.

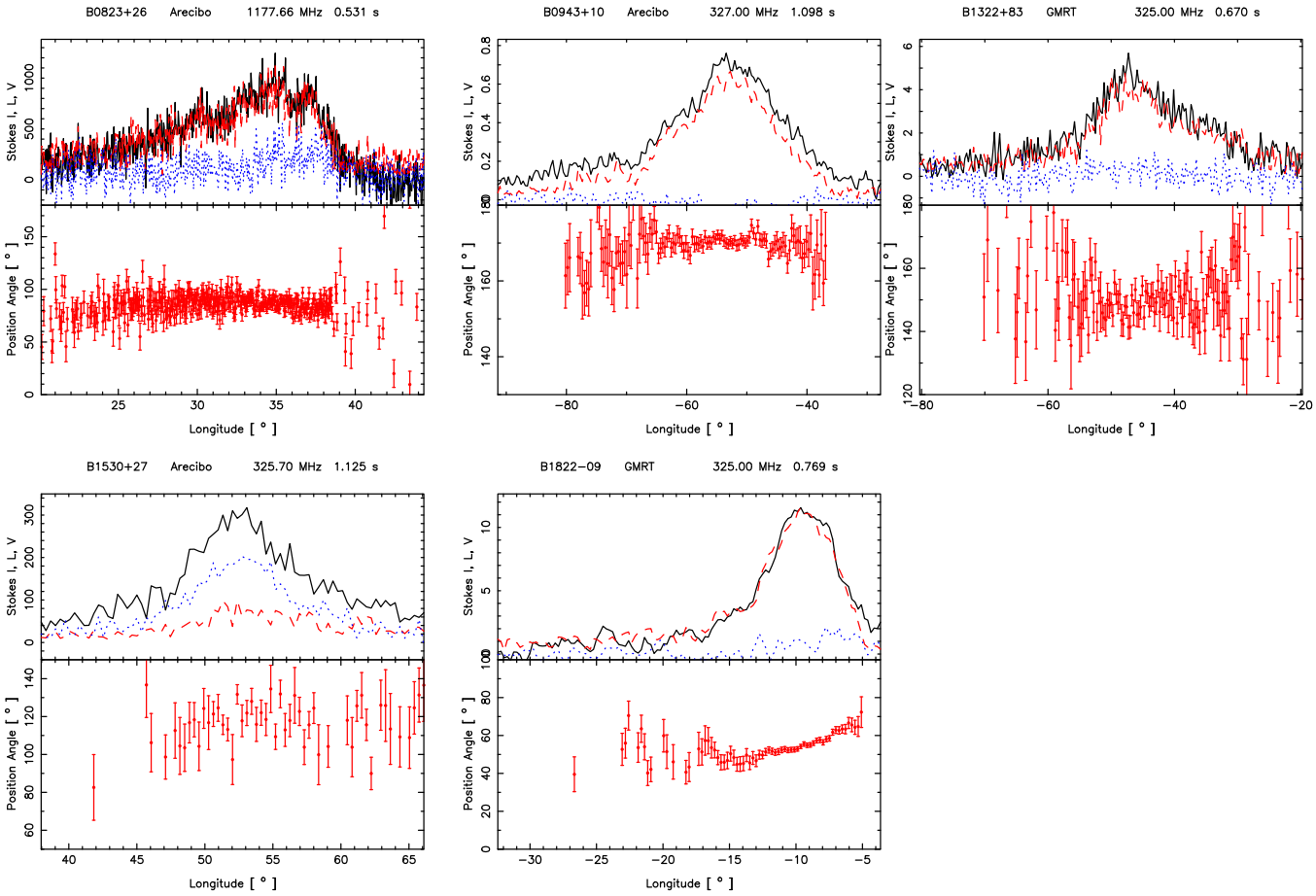

Figure 3. Polarization characteristics of pulsars with the PPC emission: total intensity I (black line), the linear polarization L (red broken line), circular polarization V (blue dotted line), as well as the polarization position angle (PPA). The postcursor in pulsar B0823+26 (top left) shows high linear polarization (>70%) and moderate circular polarization (<40%). The PPA shows no discernible swing across the postcursor feature. In B0943+10 (top center) the precursor has high linear polarization and low circular polarization with the PPA remaining flat across the precursor. In the case of the precursor in B1322+83 (top right), once again we see high linear polarization (>75%) but low circular polarization (<10%) and a flat PPA swing. Pulsar B1530+27's postcursor (bottom left) exhibits somewhat different polarization characteristics. Its linear polarization is smaller (<30%) but with large circular polarization (>70%). Its PPA swing, however, is relatively flat across the feature. The precursor in pulsar B1822−09 (bottom center) is characterized by high linear polarization (>80%) and minimal circular polarization (<10%). The PPA is relatively flat compared to the main pulse but shows a change of about 30° across the precursor.

than 70%. The PPA remains relatively flat across the PPC components compared to the swing across the main pulse. A closer look reveals the PPA to be not completely flat but shows some gentle swing with the change being as much as 20°–40° across some PPC components (see Figure 3). The high degree of linear polarization as well as the absence of orthogonal modes in the PPC emission indicate the likely source of emission to be a pure polarization mode.

For pulsar B0823+26 we are able to securely identify the alignment of the dominant postcursor polarization mode. As summarized in Rankin (2007), Morris et al. (1979) measured the absolute PPA at the peak of the star's main pulse as +48(3)° counterclockwise from north. Its proper motion direction was determined by Lyne et al. (1982) as +146(1)°. Assuming that the former reflects the "fiducial" orientation of the projected magnetic field at the axis longitude, then the latter minus the former indicates an orthogonal 98(1)° relation between the projected field orientation and the polarization of the radiation, implying that this radiation represents the extraordinary (X) propagation mode. Further, reference to the Everett & Weisberg (2001) discussion on this pulsar shows clearly that the postcursor polarization represents the same mode (X) as the peak of the main pulse.

4.2. PPC Emission in Terms of Emission Mechanisms

The absence of frequency evolution of PPC emission leads to two possibilities about its origin; either they emanate from a range of emission altitudes with no discernible frequency evolution (like in regions of the magnetosphere where the magnetic field lines do not diverge significantly with emission height) or the emission mechanism has provisions for emitting different frequencies at similar locations in the magnetosphere. Based on a number of phenomenological properties of the main pulse radio emission, the most favorable mechanism appears to be the soliton induced curvature radiation (Melikidze et al. 2000; Gil et al. 2004; Mitra et al. 2009). Here we will discuss whether the same mechanism can be applied to the PPC emission as well.

The soliton model requires the presence of a nonstationary flow of the plasma along the open magnetic field lines. The presence of an inner vacuum gap above the magnetic poles acts as a source of relativistic plasma (Ruderman & Sutherland 1975; Gil et al. 2003) comprised of singly charged primary particles (characterized by Lorentz factor $\gamma_b \sim 10^6$) and secondary pair plasma (with Lorentz factors $\gamma_p \sim 10$–1000). The nonstationary flow coupled with the spread in particle energies results in

Table 3
Conditions for Coherent Curvature Radiation in PPC Emission

Pulsar	P (s)	$\dot{P}_{-15}$ 10^{-15} s s^{-1}	B_S 10^{12} G	$\dot{E}$ 10^{31} erg s^{-1}	r_{PC} R_S	ν_p (MHz)	Equation (9) γ_p=200	γ_c	ν_c (MHz)	γ_c^{500}
B0823+26	0.531	1.71	0.96	45.2	600	21.6	0.011	10	0.001	750
B0943+10	1.098	3.49	1.98	10.4	130	213.1	0.113	45	0.559	450
B0950+08	0.253	0.23	0.24	56	70	392.8	0.209	70	1.950	350
B1322+83	0.670	0.57	0.62	7.4	75	349.8	0.185	65	2.610	375
B1524−39	2.418	19.07	6.87	5.3	110	343.7	0.182	65	1.717	425
B1530+27	1.125	0.78	0.95	2.2	550	16.7	0.009	10	0.0008	725
B1822−09	0.769	52.50	6.43	456	110	589.5	0.311	90	5.052	425
B2217+47	0.538	2.77	1.23	69.9	800	15.7	0.008	10	0.001	825

Notes. $\nu_p = \omega_p/2\pi$ and $\nu_c = \omega_c/2\pi$. The condition for coherent radio emission requires Equation (9) and $\nu_c < 2\sqrt{\gamma_p}\nu_p$. The conditions are not satisfied in all of the cases; see Section 4.2 for details.

overlapping clouds of secondary plasma. This gives rise to the two-stream instability which generates electrostatic Langmuir waves (Asseo & Melikidze 1998). The modulational instability of the Langmuir waves leads to the formation of relativistic charged solitons, which excite coherent curvature radiation in the ambient plasma. The condition for coherent emission requires the wavelength to be greater than the intrinsic soliton size (Melikidze et al. 2000), i.e.,

$$\omega < 2\sqrt{\gamma_p}\omega_p, \tag{7}$$

where $\omega_p = (4\pi e^2 n/m_e)^{1/2}$ is the plasma frequency; $n = \chi n_{GJ}$, with $\chi \sim 10^4$.

The characteristic frequency of curvature radiation is given as

$$\omega_c = \frac{3}{2}\gamma_p^3 c/R_C, \tag{8}$$

where R_C is the curvature radius of the magnetic field lines. The emission occurs at heights of $50R_S$ where the radius of curvature of dipolar magnetic field lines can be approximated as $R_C \sim 10r$, here r being the emission height. The particle energies required for emission at these heights are $\gamma_c \sim 200$. The growth of the Langmuir waves is determined by the complex frequency (Γ) where the instability can grow if the growth time ($1/\Gamma$) is much less than the characteristic time scale of the plasma cloud to overlap and interact ($1/\Gamma \ll \phi_o/c$; here $\phi_o \sim 10^5$ cm, is the length scale of secondary plasma cloud). The inequality is expressed in terms of typical pulsar parameters as (Asseo & Melikidze 1998):

$$(\gamma_p/100)^{-1.5}(r/50R_S)^{-1.5}(\dot{P}_{-15}/P)^{1/4} \gg 0.1, \tag{9}$$

where P is the pulsar period, R_S the radius of neutron star, and $\dot{P}_{-15}$ the period derivative in units of 10^{-15} s s^{-1}.

We have applied the soliton induced curvature radiation mechanism to the PPC emission in eight pulsars and the results are outlined in Table 3 along with the basic pulsar properties period, period derivative, surface magnetic field, and spin down energies. The emission heights are determined from the radii of the beam opening angles (using Equation (6)) and vary from 70–800 R_S (see Column 6 in the table), which as we mentioned earlier are lower limits. We undertake the following calculations to determine the viability of the emission mechanism for PPC components.

1. The values of the plasma frequency are determined in Column 7 for each pulsar at the emission height of the PPC components. The plasma frequencies are quite low which already makes it unlikely for the mechanism to emit higher frequencies (>1 GHz) where PPC emission is observed (see Equation (7)).
2. We checked whether the particles responsible for the main pulse emission with energies $\gamma_p \sim 200$ can give rise to the detected PPC components. The condition in Equation (9) is determined for the $\gamma_p = 200$ particles (Table 3, Column 8) and turns out to be low for optimal growth. These clearly imply that the $\gamma_p \sim 200$ particles in the secondary plasma are incapable of developing the necessary instability growth to generate coherent emission at these emission heights.
3. We next look at the particles in the secondary plasma that can give rise to optimal growth. We assumed the condition in Equation (9) to be unity and determined the particle energies that satisfy the growth condition at the PPC emission heights. The particle energies turn out to be very low, γ_c is between 10 and 100 as shown in Column 9. We have determined the frequency of curvature radiation (ν_c) at these emission heights using γ_c for each of the pulsars, and the emission frequency is very low ranging from a few kilohertz to a few megahertz—much below the observing frequency as shown in Column 10 of Table 3. This clearly indicates that the particles in the secondary plasma that are suitable for growth of instability would emit at much below observing frequencies.
4. Finally, we have calculated the particle energies that are capable of curvature radiation in the observable RF range. We took the radiation frequency as 500 MHz and using Equation (8) calculated γ_c^{500} at the heights of PPC emission. The Lorentz factors ranged from 350 to 825 as shown in the last column. Lorentz factors between 350 and 825 would violate Equation (9), and thus will not lead to coherent emission.

We have demonstrated that the soliton induced coherent curvature radiation, which is responsible for the main pulse emission, is unlikely to emit PPC components. Note that in the case of PSR B0823+26, we have explored a scenario where the PPA below the PPC as well as the main pulse can be associated with the X plasma mode, which in turn argues for a mechanism similar to curvature radiation. This issue needs further understanding which however is beyond the scope of our present studies.

There is another emission mechanism that develops in the outer magnetosphere near the light cylinder that can give rise to coherent radio emission (Kazbegi et al. 1991; Lyutikov et al. 1999). The coherent emission can be generated when the naturally developing electromagnetic modes in the clouds

of secondary plasma undergo negative absorption from the highly energetic primary particles via the cyclotron resonance instability. Recently Basu et al. (2013) have used this mechanism to explain the origin of off-pulse emission from long period pulsars. However, the mechanism suffers from concerns of cutoff frequencies and fine tuning of plasma parameters similar to the curvature emission mechanism. This scenario would further require explanation of the pulsed nature of the PPC emission and detailed studies are needed to ascertain its viability as a possible emission mechanism.

Petrova (2008) has explained the precursor emission as a result of induced scattering of the main pulse emission into the background. The scattered precursor is directed along the magnetic field and appears ahead of the main pulse due to rotational aberration. However, according to this mechanism the precursor separation does not exceed 30° in longitude for the scattering region to be within the magnetosphere. In our studies we have found precursors in pulsars B0943+10, B0950+08, B1322+83, and B1524−39 with longitudinal separation in excess of 30°. This study further does not address the presence of postcursors.

In this work we have demonstrated the PPC emission in pulsars to be different from the canonical main pulse emission. The locations of the PPC emission are higher up in the magnetosphere compared to the main pulse. It seems likely that the coherent curvature radiation mechanism for the main pulse is inadequate to explain their origin. The number of pulsars with precursor components stands at five while there are four pulsars with postcursor emission. We have also identified three potential candidates for PPC emission that we could not fully analyze due to the lack of high quality observations. Detailed studies are required to search for more PPC emission in the pulsar population and to further characterize their nature including identifying the location of the PPC emission within the magnetosphere and also looking for an emission mechanism applicable to them.

We thank the anonymous referee for useful comments. We would also like to thank Janusz Gil and Giorgi Melikidze for their comments which helped to improve the paper. This work was partially supported by the grant DEC-2013/09/B/ST9/02177 of the Polish National Science Centre. Portions of this work were carried out with support from US National Science Foundation grants 08-07691 and 09-68296. Arecibo Observatory is operated by SRI International under a cooperative agreement with the NSF, and in alliance with Ana G. Méndez-Universidad Metropolitana, and the Universities Space Research Association. We thank the staff of the GMRT that made the observations possible. GMRT is run by the National Centre for Radio Astrophysics of the Tata Institute of Fundamental Research. This work made use of the NASA ADS astronomical data system.

REFERENCES

Asseo, E., & Melikidze, G. I. 1998, MNRAS, 301, 59
Backus, I., Mitra, D., & Rankin, J. M. 2010, MNRAS, 404, 30
Basu, R., Mitra, D., & Melikidze, G. I. 2013, ApJ, 772, 86
Blaskiewicz, M., Cordes, J. M., & Wasserman, I. 1991, ApJ, 370, 643
Deshpande, A. A., & Rankin, J. M. 2001, MNRAS, 322, 438
Deich, W. T. S. 1986, M. S. thesis, Cornell Univ.
Everett, J. E., & Weisberg, J. M. 2001, ApJ, 553, 341
Gangadhara, R. T., & Gupta, Y. 2001, ApJ, 555, 31
Gil, J., Lyubarsky, Y., & Melikidze, G. I. 2004, ApJ, 600, 872
Gil, J., Melikidze, G. I., & Geppert, U. 2003, A&A, 407, 315
Gil, J. A., Gronkowski, P., & Rudnicki, W. 1984, A&A, 132, 312
Gil, J. A., Jessner, A., Kijak, J., et al. 1994, A&A, 282, 45
Gil, J. A., & Sendyk, M. 2000, ApJ, 541, 351
Gould, D. M., & Lyne, A. G. 1998, MNRAS, 301, 235
Hankins, T. H., & Fowler, L. A. 1986, ApJ, 304, 256
Hankins, T. H., & Rankin, J. M. 2010, AJ, 139, 168
Kazbegi, A. Z., Machabeli, G. Z., & Melikidze, G. I. 1991, MNRAS, 253, 377
Kijak, J., & Gil, J. 1998, MNRAS, 299, 855
Krzeszowski, K., Mitra, D., Gupta, Y., et al. 2009, MNRAS, 393, 1617
Latham, C., Mitra, D., & Rankin, J. 2012, MNRAS, 427, 180
Lorimer, D. R., Yates, J. A., Lyne, A. G., & Gould, D. M. 1995, MNRAS, 273, 411
Lyne, A. G., Anderson, B., & Salter, M. J. 1982, MNRAS, 201, 503
Lyne, A. G., & Manchester, R. N. 1988, MNRAS, 234, 477
Lyutikov, M., Blandford, R. D., & Machabeli, G. 1999, MNRAS, 305, 338
Maciesiak, K., & Gil, J. 2011, MNRAS, 417, 1444
Maciesiak, K., Gil, J., & Melikidze, G. I. 2012, MNRAS, 424, 1762
McLaughlin, M. A., & Rankin, J. M. 2004, MNRAS, 351, 808
Melikidze, G. I., Gil, J. A., & Pataraya, A. D. 2000, ApJ, 544, 1081
Mitra, D., & Deshpande, A. A. 1999, A&A, 346, 906
Mitra, D., Gil, J., & Melikidze, G. I. 2009, ApJ, 696, 141
Mitra, D., & Li, X. H. 2004, A&A, 421, 215
Mitra, D., & Rankin, J. M. 2002, ApJ, 577, 322 (ET IX)
Mitra, D., & Rankin, J. M. 2011, ApJ, 727, 92 (ET IX)
Morris, D., Graham, D. A., Sieber, W., et al. 1979, A&A, 73, 46
Petrova, S. A. 2008, MNRAS, 384, L1
Radhakrishnan, V., & Cooke, D. J. 1969, Aph. Lett, 3, 225
Rankin, J. M. 1983, ApJ, 274, 333 (ET I)
Rankin, J. M. 1990, ApJ, 352, 247 (ET V)
Rankin, J. M. 1993a, ApJ, 405, 285 (ET VIa)
Rankin, J. M. 1993b, ApJS, 85, 145 (ET VIb)
Rankin, J. M. 2007, ApJ, 664, 443
Rankin, J. M., & Rathnasree, N. 1995, JAPA, 16, 327
Rankin, J. M., & Rathnasree, N. 1997, JAPA, 18, 91
Rankin, J. M., Suleymanova, S. A., & Deshpande, A. A. 2003, MNRAS, 340, 1076
Ruderman, M. A., & Sutherland, P. G. 1975, ApJ, 196, 51
Seiradakis, J. H., Gil, J. A., Graham, D. A., et al. 1995, A&AS, 111, 205
Suleymanova, S. A., & Shitov, Y. P. 1994, ApJ, 422, 17
von Hoensbroech, A. 1999, PhD thesis, Univ. Bonn
Weisberg, J. M., Cordes, J. M., Kuan, B., et al. 2004, ApJS, 150, 317
Weisberg, J. M., Cordes, J. M., Lundgren, S. C., et al. 1999, ApJS, 121, 171